

High-resolution Depth Maps Imaging via Attention-based Hierarchical Multi-modal Fusion

Zhiwei Zhong, Xianming Liu, *Member, IEEE*, Junjun Jiang, *Member, IEEE*, Debin Zhao, *Member, IEEE*, Zhiwen Chen, *Member, IEEE*, Xiangyang Ji, *Member, IEEE*

Abstract—Depth map records distance between the viewpoint and objects in the scene, which plays a critical role in many real-world applications. However, depth map captured by consumer-grade RGB-D cameras suffers from low spatial resolution. Guided depth map super-resolution (DSR) is a popular approach to address this problem, which attempts to restore a high-resolution (HR) depth map from the input low-resolution (LR) depth and its coupled HR RGB image that serves as the guidance. The most challenging problems for guided DSR are how to correctly select consistent structures and propagate them, and properly handle inconsistent ones. In this paper, we propose a novel attention-based hierarchical multi-modal fusion (AHMF) network for guided DSR. Specifically, to effectively extract and combine relevant information from LR depth and HR guidance, we propose a multi-modal attention based fusion (MMAF) strategy for hierarchical convolutional layers, including a feature enhance block to select valuable features and a feature recalibration block to unify the similarity metrics of modalities with different appearance characteristics. Furthermore, we propose a bi-directional hierarchical feature collaboration (BHFC) module to fully leverage low-level spatial information and high-level structure information among multi-scale features. Experimental results show that our approach outperforms state-of-the-art methods in terms of reconstruction accuracy, running speed and memory efficiency.

Index Terms—depth map super-resolution, multi-modal attention, bi-directional feature propagation.

I. INTRODUCTION

Depth information plays a critical role in a myriad of applications such as autonomous driving [2], virtual reality [3], 3D reconstruction [4] and scene understanding [5]. In recent years, with the progress of sensing technology, depth map can be readily captured by consumer-grade depth cameras such as Time-of-Flight (ToF) and Microsoft Kinect. However, the depth map taken from these commercialized cameras usually suffers from low-resolution, which hinders the subsequent depth based applications. Therefore, depth map super-resolution (DSR) has raised a lively interest in the communities of academia and industry.

DSR is inherently an ill-posed problem, as there exist multiple high-resolution (HR) depth maps corresponding to the

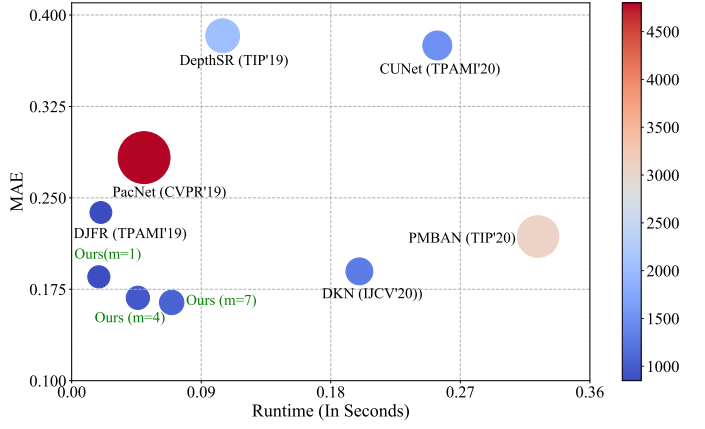


Fig. 1. Comparison of state-of-the-art methods for 4x DSR on Middlebury [1] dataset in terms of MAE (the lower the better), running time and peak GPU memory consumption that is indicated by radius of circles. Our method includes three cases with different m , which refers to the number of layers for multi-modal feature fusion. The experiments are evaluated on NVIDIA 1080ti GPU with depth map size 480x640.

same low-resolution (LR) degradation. To solve this inverse problem, one popular approach is guided DSR, considering that in practice many smartphones and robots are equipped with a conventional RGB camera as well as a depth camera. The former acquires intensity image with higher spatial resolution than depth map. Since the targets they shoot are the same scene, it is thus natural to enhance the resolution of depth by transferring structure from the HR guidance image. Specifically, guided DSR aims to apply HR guidance image as a prior for reconstructing regions in depth where there is semantically-related and structure-consistent content, and fall back to a plausible reconstruction for regions in depth with inconsistent content of the guidance.

To achieve this goal, two major problems should be carefully addressed. Firstly, it is challenging to select reference structures and propagate them properly by defining hand-crafted rules based on similarity metrics. Secondly, the guidance based approach makes a basic assumption that guidance image should contain correct mutual structural information. However, the guidance could be insufficient, or even wrong locally. It is challenging to handle the structure inconsistency problem. For regions with inconsistent structures, it is expected that guidance based approach could reduce wrong influence of the guidance and predict HR reconstruction properly.

For the first issue, data-driven based strategies have been proposed to remedy the difficulty of hand-crafted design. For

This work was supported by XX.

Z. Zhong, X. Liu, J. Jiang and D. Zhao are with the School of Computer Science and Technology, Harbin Institute of Technology, Harbin 150001, China, and also with the Peng Cheng Laboratory, Shenzhen 518052, China. E-mail: {csxm,jiangjunjun}@hit.edu.cn

Z. Chen is with Taobao (China) Software Co.,Ltd., Beijing, China. E-mail: zhiwen.czw@alibaba-inc.com

X. Ji is with the Department of Automation, Tsinghua University, Beijing 100084, China. E-mail: xyji@tsinghua.edu.cn

instance, Hui *et al.* [6] proposed a multi-scale guided convolutional network (DMSG) for DSR, which complemented LR depth features with HR intensity features using a progressively hierarchical fusion strategy. Similarly, in [7], Guo *et al.* proposed a DSRNet to infer a HR depth map from its LR version by hierarchical features driven residual learning. Su *et al.* [8] proposed a pixel-adaptive convolution based network (PacNet), which is actually a fine-grained filtering operation that can effectively learn to leverage guidance information. Similar strategy that uses pixel-wise transformation also appears in [9]. The work [10] presented a progressive multi-branch aggregation network (PMBAN) for depth SR, which consisted of stacked multi-branch aggregation blocks to progressively recover the degraded depth map.

For the second issue, recent efforts focus on learning based selection strategy for the common structures existing in both the target and guidance images. For instance, Li *et al.* [11] proposed a joint image filtering with deep convolutional networks, which can selectively transfer salient structures that are consistent with multi-modal inputs. The network architecture of DKN [12] is similar to DJFR [11], but contains a weight and offset learning module to explicitly learn sparse and spatially-variant kernels. Recently, Deng *et al.* [13] proposed a common and unique information splitting network (CUNet) to automatically determine the common information shared among different modalities, according to which an adaptive fusion operation was performed.

Although significant progress has been achieved, deep learning based DSR is still an open problem. The key challenge is how to achieve a good balance among performance, running time and network complexity, so as to promote its usage in practical scenarios. In this paper, we embrace this challenge and propose a novel attention-based hierarchical multi-modal fusion (AHMF) network to perform structure selection, propagation and prediction simultaneously for guided DSR. Specifically, to effectively extract and combine relevant information from LR depth and HR guidance, we propose a multi-modal attention based fusion (MMAF) for hierarchical convolutional layers. It consists of a feature enhancement block that is tailored to adaptively select useful information and filter out unwanted ones, such as texture information in guidance and noise in depth that would disturb the depth reconstruction; and a feature recalibration block that is designed to adaptively rescale enhanced features to unify the similarity metrics of modalities with different appearance characteristics. Furthermore, considering that in CNN shallower layers encode rich spatial details but lack semantic knowledge while deeper layers are more effective to capture high-level context and structure information but lose spatial information, we propose a bi-directional hierarchical feature collaboration (BHFC) module to fully leverage the hierarchical fused features. Experimental results demonstrate that our method achieves superior performance than the state-of-the-arts. As shown in Fig. 1, our scheme achieves better DSR performance, faster running speed and moderate memory consumption over state-of-the-art methods.

The remainder of this paper is organized as follows. Section II reviews related work in the literature. Section III introduces

the overview of the proposed method. Then, we elaborate on the proposed multi-modal attention based fusion in Section IV and hierarchical feature collaboration strategy in Section V. Extensive experimental results are presented in Section VI. Finally, Section VII concludes this paper.

II. RELATED WORK

A. Guided Depth Super-resolution

In the literature, many works have been developed for guided DSR, which can be roughly divided into three categories: filtering based, optimization based and deep learning based. The filtering based approaches, such as [14], [15], reconstruct the depth map in the means of weighted average of target image values with a local filter. Though these filtering based methods are at low computational cost, they cannot maintain the global information as the weights of filter are calculated by the local content in the guidance image. This would inevitably transfer inaccurate structures to the depth image when the assumption of structure similarity is invalid. Different from filtering based methods, optimization based methods formulate depth image super-resolution as a global optimization problem. They adopt various priors to constrain the high-dimensional solution space for this ill-posed problem. For example, Ferstl *et al.* [16] formulated the DSR problem as a convex optimization problem and employed a high-order Total Generalized Variation (TGV) regularization to get a piecewise smooth solution. Liu *et al.* [17] proposed a DSR method by combining both internal and external priors formulated in the graph domain. However, these hand-crafted priors suffer from limitations in modeling the real world image degradation process. Moreover, solving the optimization problem is usually time-consuming due to the iterative computation process.

Based on U-Net architecture, Guo *et al.* [18] proposed a hierarchical feature driven network and they claimed that their network could make full use of features extracted from depth and guided image compared to the existing methods. Kim *et al.* [12] proposed a deformable kernel network for depth SR, they employed the kernel based method but the weights and offsets of the kernel were learned by the network automatically. Su *et al.* [8] argued that the convolutional operation was content-agnostic and proposed a pixel-adaptive convolution to address this problem, and they conducted plenty of experiments to show that their method could easily adapt to a lot of applications such as joint upsampling, semantic segmentation and CRF inference.

B. Attention Model

Attention mechanism has shown remarkable performance in deep convolutional neural network and has been introduced in a large number of computer computer vision tasks. Zhang *et al.* [19] proposed a self-attention based GAN architecture for image generation problem, experimental results showed that the self-attention module could effectively capture long-range dependencies. Inspired by the non-local mean method, Wang *et al.* [20] proposed a non-local neural network for video classification and the self-attention could be viewed

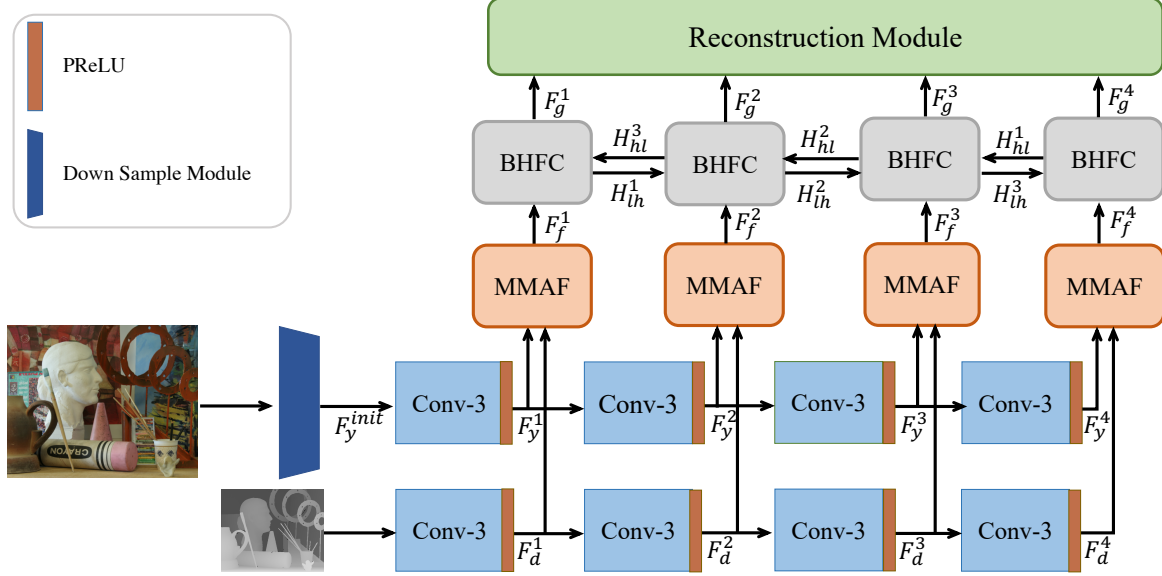


Fig. 2. The network architecture of our proposed attention-based hierarchical multi-modal fusion (AHMF) network, where MMAF represents the proposed multi-modal attention based fusion module and BHFC represents the bi-directional hierarchical feature collaboration module.

as a special case of it. Hu *et al.* [21] proposed a squeeze-and-excitation module to let the network pay more attention to important feature maps by explicitly modelling channel-wise interrelations. Li *et al.* [22] proposed a selective kernel network (SKNet) to let the neural adjust its receptive field adaptively. Mei *et al.* [23] proposed a pyramid attention module for image restoration, their method could capture long range correspondences in a multi-level fashion. To accelerate the channel attention and decrease the model complexity, Wang *et al.* [24] replaced the fully connected layer used in channel attention module with a 1D convolution. Yu *et al.* [25] proposed a gated convolution to solve the problem of traditional convolutional layer treating all input pixel equally for free-from image inpainting tasks, then Chang *et al.* [26] extended the 2D gated convolution to 3D part for free-from video inpainting. Among these works, the most related to our method is [22], however, there are still some differences between them, firstly the feature recalibration block in our method is to rescale the different modal data while [22] aims to dynamically select receptive field for each neurons. Secondly, we use mean and standard deviation pooling instead of max pooling used in [22] to get global embedding, which is more suitable for low-level vision.

C. Multi-level Feature Fusion

In deep convolutional networks, the features of shallower layers usually contain low-level details while the ones of deeper layers are composed of high-level semantic information. In order to make the best use of both high and low level features, enormous methods are proposed. He *et al.* [27] introduced a skip-connection which was also called residual learning operator for training very deep convolutional networks, with the help of this operation the deeper layer can directly access the low-level features. Instead of pixel-wise ad-

dition, Huang *et al.* [28] concatenated the low-level and high-level features to fuse the multi-level features. Gu *et al.* [29] proposed a self-guided network for image denoising, they used high-level feature to progressively guide the low-level feature, which could enlarge the receptive field of shallower layer and enhance the network represent capability. Lin *et al.* [30] proposed a refinement network in which the low-level features was refined by the high-level semantic levels. Though the performance of the network is greatly improved, there are still some problems, for example, in [27] and [28] the low-level features cannot directly contact with high-level information due to the feed-forward nature of convolutional neural network, on the contrary, in the methods of [30] and [29] only the low-level features can be refined by the high-level features. To solve these problems, in this paper, we propose a bi-directional hierarchical feature collaboration module, in which the low-level feature and high-level can propagate to each other effectively.

III. OVERVIEW OF THE PROPOSED METHOD

In this section, we provide an overview about the proposed attention-based hierarchical multi-modal fusion network.

The pipeline of our network is illustrated in Fig. 2, consisting of five major modules that are marked by different colors: 1) module of guidance image downsampling; 2) module of feature extraction; 3) module of multi-modal attention based fusion (MMAF); 4) module of bi-directional hierarchical feature collaboration (BHFC) and 5) module of final HR depth reconstruction. The main technical contributions of our proposed scheme are the MMAF and BHFC modules, which are elaborated in Section IV and V respectively.

Specifically, the proposed network takes a LR depth map $D_{LR} \in \mathbb{R}^{H \times W \times 1}$ and a HR guidance image $Y \in \mathbb{R}^{\alpha H \times \alpha W \times C}$ as inputs, where α is the upscale factor, H, W and C represent height, width and the number of channels

respectively. Considering that the resolution of guidance \mathbf{Y} is higher ($\alpha \times$) than the corresponding depth \mathbf{D}_{LR} , to facilitate the subsequent processing, we need to downsample \mathbf{Y} to achieve resolution consistency. Instead of using traditional downsampling strategy such as bicubic, which would result in information loss, we propose to leverage inverse pixel-shuffle [31] to progressively downsample \mathbf{Y} with the upscale factor α . In this way, it can not only preserve all the original information of \mathbf{Y} but also achieve resolution balance of two inputs. More specifically, taking $\alpha = 4$ as an example, \mathbf{Y} needs to be downsampled by 2 ($\log_2 \alpha$) times:

$$\mathbf{F}_y^{init} = \text{Down}(\sigma(\mathbf{W} * \text{Down}(\mathbf{Y}) + b)), \quad (1)$$

where $\text{Down}(\cdot)$ represents the inverse pixel-shuffle operator with downscale factor 2; \mathbf{W} is a 1×1 convolutional kernel; b is the bias term; $*$ means convolutional operation; σ represents a Parametric Rectified Linear Unit (PReLU) [32] activation function.

We then adopt a multi-level fashion to fully extract meaningful features from both depth and guidance:

$$\mathbf{F}_d^1 = \sigma(\mathbf{W}_d^1 * \mathbf{D}_{LR} + b_d^1), \quad (2)$$

$$\mathbf{F}_y^1 = \sigma(\mathbf{W}_y^1 * \mathbf{F}_y^{init} + b_y^1), \quad (3)$$

$$\mathbf{F}_d^i = \sigma(\mathbf{W}_d^i * \mathbf{F}_d^{i-1} + b_d^i), 1 < i \leq m, \quad (4)$$

$$\mathbf{F}_y^i = \sigma(\mathbf{W}_y^i * \mathbf{F}_y^{i-1} + b_y^i), 1 < i \leq m, \quad (5)$$

where \mathbf{W}_d^i and \mathbf{W}_y^i are 3×3 convolutional kernels of i -th layer that are used for depth and guidance feature extraction respectively; b_d^i and b_y^i are the bias terms; m refers to the number of layers for multi-modal feature extraction.

After extracting multi-modal features, the following question is how to fuse them for HR depth reconstruction. We do this by the proposed multi-modal attention based fusion (MMAF):

$$\mathbf{F}_f^i = \text{MMAF}_i(\mathbf{F}_y^i, \mathbf{F}_d^i), 1 \leq i \leq m, \quad (6)$$

which considers the difference between guidance and depth and adaptively combines multi-modal features by the attention mechanism. In this way, it optimally preserves consistent structures and suppresses inconsistent components in a learning manner. Followed by MMAF is the proposed bi-directional hierarchical feature collaboration (BHFC), which is tailored to further jointly leverage low-level spatial and high-level semantic information:

$$\mathbf{F}_g^i = \text{BHFC}_i([\mathbf{F}_f^i, \mathbf{H}_{lh}^{i-1}, \mathbf{H}_{hl}^{m-i}]), 1 \leq i \leq m, \quad (7)$$

where \mathbf{H} is hidden state and the subscripts lh and hl denote the information propagation direction. \mathbf{H}^0 is the initial state and is set as zero.

Finally, with the refined features $\{\mathbf{F}_g^i\}_{i=1}^m$, we arrive at the HR depth reconstruction module, which produces the upsampled depth image by pixel-shuffle [33]:

$$\mathbf{D}_{SR} = \text{Up}(\mathbf{W} * [\mathbf{F}_g^1, \mathbf{F}_g^2, \dots, \mathbf{F}_g^m] + b) + \mathbf{D}_{LR}^\uparrow, \quad (8)$$

where \mathbf{W} and b are the weight and bias of a 1×1 convolutional layer for channel reduction; $\text{Up}(\cdot)$ is denoted as the pixel-shuffle operation; $[\cdot]$ is used to concatenate the refined features;

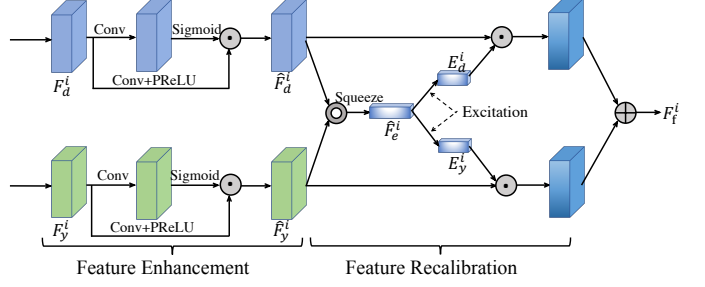


Fig. 3. Multi-modal attention based fusion (MMAF), where \odot is pixel-wise multiplication, \oplus is pixel-wise summation and \odot denotes concatenation. The MMAF takes extracted depth and guidance features as inputs and outputs the fused multi-modal features.

\mathbf{D}_{LR}^\uparrow is the bicubic upsampled version of the input LR depth image; $\mathbf{D}_{SR} \in \mathbb{R}^{\alpha H \times \alpha W \times 1}$ is the final reconstructed HR depth image.

The network is trained using the following loss function:

$$L(\theta) = \frac{1}{N} \sum_{i=1}^N \|\mathcal{F}(\mathbf{D}_{LR}, \mathbf{Y}; \theta) - \mathbf{D}_{GT}\|_1, \quad (9)$$

where $\mathcal{F}(\cdot)$ represents the overall network architecture and θ are network parameters. \mathbf{D}_{GT} is the ground-truth HR depth map, N is the number of training samples.

IV. MULTI-MODAL ATTENTION BASED FUSION

In this section, we introduce the proposed multi-modal attention based fusion strategy in detail. In guided DSR, the core is the act of extracting and combining relevant information from LR depth and HR guidance so as to derive superior performance over using only depth. One can perform concatenation or summation of outputs of two separate branches for depth and guidance respectively, and then use uni-modal CNNs to get the final reconstruction, as done in [11]. Some works suggest mid-level feature fusion could benefit reconstruction. For instance, [6], [7], [10] propose to fuse hierarchical features of convolutional layers of two branches, which is still conducted by concatenation. However, intermediate level features of depth and guidance have different semantic meanings, making the intermediate fusion more challenging. The simple concatenation is not effective for this purpose.

Different from existing guided DSR methods, we propose to hierarchically combine multi-modal features by attention mechanism. We attempt to preserve consistent structures and suppress inconsistent components in a learning manner. As shown in Fig. 3, our proposed fusion scheme consists of a feature enhancement block and a feature recalibration block, which are elaborated in the following.

Feature Enhancement Block: The guidance image contains rich texture information, which would disturb the depth reconstruction, while depth itself contains noise due to the limitation of sensors. In view of these, we propose to leverage feature enhancement block (FEB) to adaptively select useful information and filter out unwanted one. Specifically, inspired by [25], we leverage gated units as the FEB. Given the

extracted multi-modal features \mathbf{F}_d^i and \mathbf{F}_y^i ($1 \leq i \leq m$) as inputs, the process of FEB can be formulated as follows:

$$\hat{\mathbf{F}}_d^i = \sigma(\mathbf{W}_{d,1}^i * \mathbf{F}_d^i + b_{d,1}^i) \odot \phi(\mathbf{W}_{d,2}^i * \mathbf{F}_d^i + b_{d,2}^i), \quad (10)$$

$$\hat{\mathbf{F}}_y^i = \sigma(\mathbf{W}_{y,1}^i * \mathbf{F}_y^i + b_{y,1}^i) \odot \phi(\mathbf{W}_{y,2}^i * \mathbf{F}_y^i + b_{y,2}^i), \quad (11)$$

where $\mathbf{W}_{d,1}^i$, $\mathbf{W}_{d,2}^i$ and $\mathbf{W}_{y,1}^i$, $\mathbf{W}_{y,2}^i$ are convolutional kernels for depth and guidance respectively, the subscripts 1 and 2 represent two different convolutional operations; $b_{d,1}^i$, $b_{d,2}^i$ and $b_{y,1}^i$, $b_{y,2}^i$ are the corresponding bias terms; \odot denotes element-wise multiplication; ϕ is sigmoid function to limit the output of the gating operation within the range of 0 and 1; σ is PReLU activation function; $\hat{\mathbf{F}}_d^i$ and $\hat{\mathbf{F}}_y^i$ are enhanced features of depth and guidance respectively.

Feature Recalibration Block: Considering depth and guidance images exhibit notably different appearance characteristics due to the difference in imaging principle, similar pixels in guidance image may have quite different values in depth and vice versa. To unify the similarity metrics, we employ multi-modal feature recalibration block (FRB) to recalibrate the enhanced multi-modal features by FEB. The FRB consists of two units: *multi-modal feature squeeze unit*, which is tailored to learn global joint knowledge from all modalities, and *feature excitation unit*, which uses the learned joint knowledge to adaptively emphasize useful features for each modal. Specifically, the multi-modal squeeze unit can be formulated as follows:

$$\hat{\mathbf{F}}_c^i = \sigma(\mathbf{W}_c^i * ([\hat{\mathbf{F}}_d^i, \hat{\mathbf{F}}_y^i]) + b_c^i), \quad (12)$$

$$\hat{\mathbf{F}}_e^i = \text{AvgPool}(\hat{\mathbf{F}}_c^i) + \text{StdPool}(\hat{\mathbf{F}}_c^i), \quad (13)$$

where $[\cdot, \cdot]$ denotes concatenation operation; \mathbf{W}_c^i is a 3×3 convolutional kernel; AvgPool(\cdot) and StdPool(\cdot) mean average pooling and standard deviation pooling respectively. $\hat{\mathbf{F}}_e^i$ is the global joint knowledge learned from all modalities, which is further fed into the feature excitation unit:

$$\mathbf{E}_d^i = \sigma(\mathbf{W}_d^i * \hat{\mathbf{F}}_e^i + b_d^i), \quad (14)$$

$$\mathbf{E}_y^i = \sigma(\mathbf{W}_y^i * \hat{\mathbf{F}}_e^i + b_y^i), \quad (15)$$

$$\mathbf{F}_f^i = \mathbf{E}_d^i \odot \hat{\mathbf{F}}_d^i + \mathbf{E}_y^i \odot \hat{\mathbf{F}}_y^i, \quad (16)$$

where \mathbf{W}_d^i , \mathbf{W}_y^i and b_d^i , b_y^i are 1×1 convolutional kernels and bias terms for depth and guidance respectively; σ is the PReLU activation function; \mathbf{E}_d^i and \mathbf{E}_y^i are the excitation signals for depth feature and guidance feature respectively; \mathbf{F}_f^i denotes the fused multi-modal feature.

V. HIERARCHICAL FEATURE COLLABORATION

It is known that in CNN shallower layers encode rich spatial details but lack semantic knowledge, while deeper layers are more effective to capture high-level context and structure information but lose spatial information. Motivated by this observation, we argue that low-level spatial details and high-level structure information should collaborate to boost by each other. Accordingly, we propose a bi-directional hierarchical feature collaboration (BHFC) module to fully leverage the hierarchical fused features.

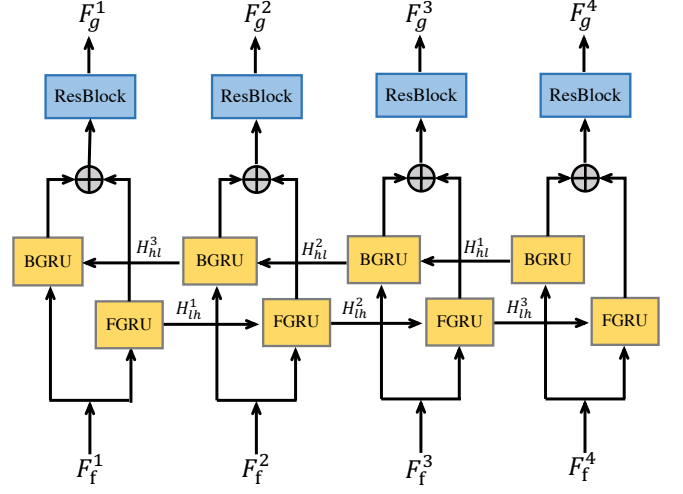


Fig. 4. Hierarchical feature collaboration with four BHFCs, where \oplus means pixel-wise summation. It takes the fused multi-modal features as inputs and sends them to a bi-directional GRU for multi-level features propagation and refinement.

Specifically, as shown in Fig. 4, we propose to use bi-directional convolutional gated recurrent units (GRU) for hierarchical feature collaboration by propagating information from one layer to all the other layers. BHFC takes the fused multi-modal features $\{\mathbf{F}_f^1, \dots, \mathbf{F}_f^m\}$ as inputs. Without loss of generality, we take the i -th input \mathbf{F}_f^i as an example. It is processed by forward GRU (FGRU) and backward GRU (BGRU), whose results are added together and passed through a residual block [34] for further boosting the hierarchical features. This procedure is formulated as follows:

$$\mathbf{F}_g^i = \text{Res}(\text{FGRU}(\mathbf{F}_f^i, \mathbf{H}_{lh}^{i-1}) + \text{BGRU}(\mathbf{F}_f^i, \mathbf{H}_{hl}^{m-i})), \quad (17)$$

where $\text{Res}(\cdot)$ represents a residual block; \mathbf{H}_{lh} and \mathbf{H}_{hl} are the hidden states of FGRU and BGRU respectively. The mathematical model of FGRU can be formulated as follows:

$$\mathbf{Z}_{lh}^i = \sigma(\mathbf{W}_z^i * [\mathbf{H}_{lh}^{i-1}, \mathbf{F}_f^i] + b_z^i), \quad (18)$$

$$\mathbf{R}_{lh}^i = \sigma(\mathbf{W}_r^i * [\mathbf{H}_{lh}^{i-1}, \mathbf{F}_f^i] + b_r^i), \quad (19)$$

$$\hat{\mathbf{H}}_{lh}^i = \tanh(\mathbf{W}_h^i * [\mathbf{R}_{lh}^i \odot \mathbf{H}_{lh}^{i-1}, \mathbf{F}_f^i] + b_h^i), \quad (20)$$

$$\mathbf{H}_{lh}^i = \mathbf{Z}_{lh}^i \odot \hat{\mathbf{H}}_{lh}^i + (1 - \mathbf{Z}_{lh}^i) \odot \mathbf{H}_{lh}^{i-1}, \quad (21)$$

where \mathbf{W} denotes 3×3 convolutional kernel, the subscripts of which represent different convolutional layers; b is the bias term; \mathbf{Z}_{lh}^i , \mathbf{R}_{lh}^i and \mathbf{H}_{lh}^i represent update gate, reset gate and hidden states respectively. We set the initial states to zero. BGRU(\cdot) is with the same formulation as FGRU(\cdot). FGRU(\cdot) controls the information flow from low-to-high layers, while BGRU(\cdot) does it from high-to-low layers.

VI. EXPERIMENTS

In this section, we conduct comprehensive analysis and evaluation of our method. Firstly, we introduce the experiment settings. Then we compare our method with the state-of-the-art depth image SR methods. Finally, ablation studies are presented to investigate the effectiveness of each module proposed in our method.

TABLE I

MAE PERFORMANCE COMPARISON FOR SCALE FACTORS $4\times$, $8\times$ AND $16\times$ WITH BICUBIC DEGRADATION ON MIDDLEBURY DATASET. THE BEST PERFORMANCE IS SHOWN IN **BOLD** AND SECOND BEST PERFORMANCE IS THE UNDERSCORED ONES (LOWER MAE VALUES, BETTER PERFORMANCE).

Method	Reference	Art			Books			Dools			Laundry			Mobeius			Reindeer		
		4 \times	8 \times	16 \times	4 \times	8 \times	16 \times	4 \times	8 \times	16 \times	4 \times	8 \times	16 \times	4 \times	8 \times	16 \times	4 \times	8 \times	16 \times
Bicubic	-	1.15	2.15	4.04	0.41	0.72	1.32	0.44	0.76	1.31	0.65	1.17	2.17	0.41	0.76	1.37	0.66	1.16	2.26
ATGV [35]	ECCV'16	0.65	0.81	1.42	0.43	0.51	0.79	0.41	0.52	0.56	0.37	0.89	0.94	0.38	0.45	0.80	0.41	0.58	1.01
DMSG [6]	ECCV'16	0.46	0.76	1.53	0.15	0.41	0.76	0.25	0.51	0.87	0.30	0.46	1.12	0.21	0.43	0.76	0.31	0.52	0.99
DGDIE [36]	CVPR'17	0.48	1.20	2.44	0.30	0.58	1.02	0.34	0.63	0.93	0.35	0.86	1.56	0.28	0.58	0.98	0.35	0.73	1.29
DSRNet [7]	TIP'19	0.66	1.27	2.41	0.26	0.48	0.86	0.29	0.53	0.90	0.39	0.73	1.36	0.27	0.49	0.90	0.43	0.75	1.23
CCFN [37]	TIP'19	0.43	0.72	1.50	0.17	0.36	0.69	0.25	0.46	0.75	0.24	0.41	0.71	0.23	0.39	0.73	0.29	0.46	0.95
GSPRT [9]	ICCV'19	0.48	0.74	1.48	0.21	0.38	0.76	0.28	0.48	0.79	0.33	0.56	1.24	0.24	0.49	0.80	0.31	0.61	1.07
DJFR [11]	TPAMI'19	0.33	0.71	1.72	0.19	0.38	0.78	0.25	0.44	0.79	0.22	0.50	1.12	0.20	0.38	0.76	0.24	0.45	0.96
PacNet [8]	CVPR'19	0.40	0.82	1.59	0.22	0.49	0.84	0.28	0.53	0.85	0.28	0.56	1.08	0.23	0.44	0.79	0.29	0.53	1.00
CUNet [13]	TPAMI'20	0.47	1.06	2.34	0.33	0.63	1.41	0.40	0.67	1.27	0.41	0.80	1.88	0.29	0.65	1.12	0.35	0.69	1.14
MDAR [1]	TMM'20	0.46	0.62	1.87	0.24	0.37	0.73	0.29	0.51	0.79	0.32	0.53	1.11	0.19	0.37	0.74	0.41	0.55	0.95
PMBAN [10]	TIP'20	0.28	0.55	<u>1.11</u>	0.19	<u>0.30</u>	0.53	0.23	<u>0.37</u>	0.64	0.21	<u>0.36</u>	0.74	0.18	<u>0.31</u>	0.57	0.22	0.39	0.75
DKN [12]	IJCV'20	<u>0.25</u>	<u>0.51</u>	1.22	<u>0.16</u>	<u>0.30</u>	<u>0.52</u>	<u>0.21</u>	<u>0.35</u>	<u>0.61</u>	<u>0.17</u>	<u>0.34</u>	0.81	<u>0.16</u>	<u>0.28</u>	<u>0.54</u>	<u>0.20</u>	<u>0.38</u>	<u>0.70</u>
AHMF	Ours	0.22	0.50	1.04	0.14	0.30	0.50	0.18	0.35	<u>0.62</u>	0.15	0.34	0.73	0.14	0.28	0.53	0.18	0.37	0.64

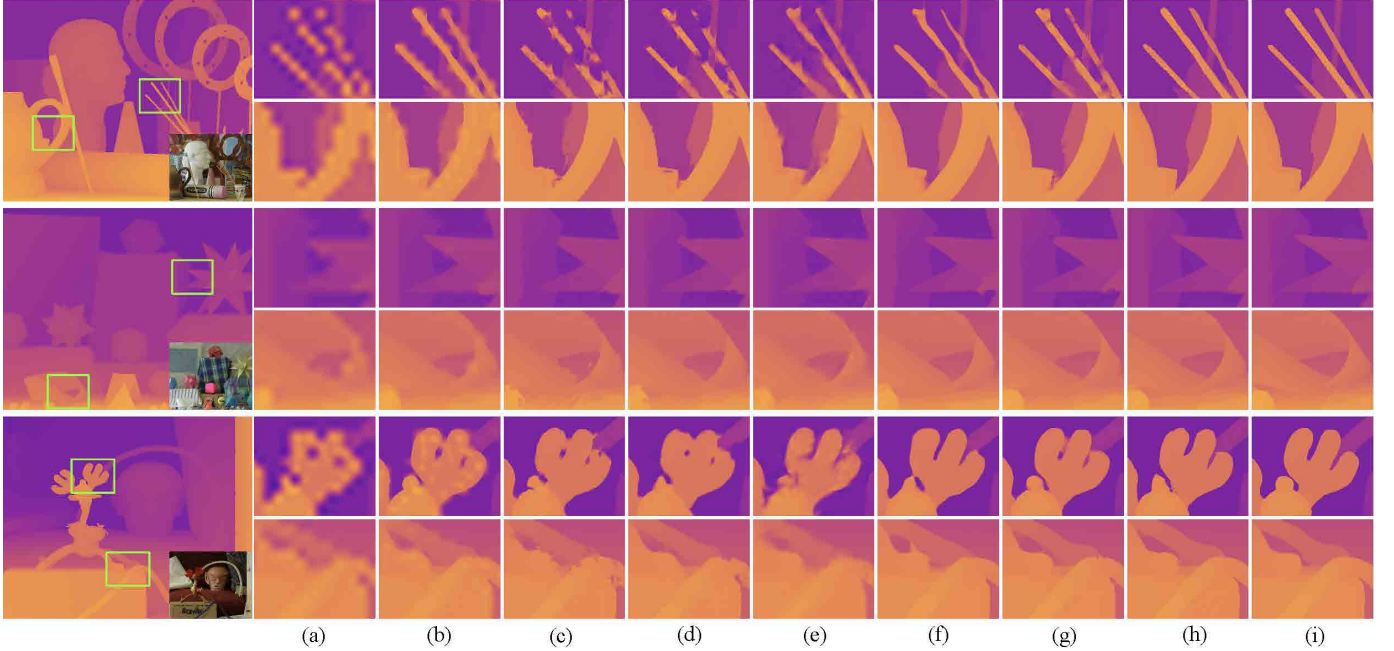


Fig. 5. Visual comparison of $16\times$ upsampling results on *Art*, *Mobeius* and *Reindeer* from Middlebury dataset [38]: (a): Bicubic, (b): DSRNet [7], (c): DJFR [11], (d): PacNet [8], (e): CUNet [13], (f): PMBAN [10], (g): DKN [12], (h): Ours, (i): GT. Please enlarge the PDF for more details.

A. Datasets and Metrics

We conduct experiments on two widely used dataset: Middlebury [38] and NYU v2 [40]. For Middlebury dataset, we follow the same experimental setting as [6]: 58 RGB-D images are collected from MPI Sintel depth dataset [41] and 34 RGB-D images from Middlebury dataset 2001 [42], 2006 [1] and 2014 [43], which serve as the training set. Our model is tested on 6 images (*Art*, *Books*, *Dools*, *Laundry*, *Mobeius*, *Reindeer*) from Middlebury [38] dataset. In order to evaluate the generalization ability cross dataset, we also test our model on Lu dataset [44]. For NYU v2 dataset, our experimental configuration is similar to [11]. The first 1000 RGB-D images are used for training and the remained 449 RGB-D images

for testing our model. To show the robustness of the proposed method, we also conduct experiments on depth maps which are captured by different sensors, such as Lu dataset [44] and Middlebury dataset [38].

Following [6], [10]–[12], [37], we use Mean Absolute Error (MAE) and root mean squared error (RMSE) to evaluate the objective performance:

$$MAE(\mathbf{D}_{GT}, \mathbf{D}_{SR}) = |\mathbf{D}_{GT} - \mathbf{D}_{SR}|, \quad (22)$$

$$RMSE(\mathbf{D}_{GT}, \mathbf{D}_{SR}) = \sqrt{\sum \frac{(\mathbf{D}_{GT} - \mathbf{D}_{SR})^2}{N}}, \quad (23)$$

TABLE II

MAE PERFORMANCE COMPARISON FOR SCALE FACTORS $4\times$, $8\times$ AND $16\times$ WITH BICUBIC DEGRADATION ON SYNTHETIC NOISY MIDDLEBURY DATASET. THE BEST PERFORMANCE IS SHOWN IN **BOLD** AND SECOND BEST PERFORMANCE IS THE UNDERSCORED ONES (LOWER MAE VALUES, BETTER PERFORMANCE).

Method	Art			Books			Dools			Laundry			Mobeius			Reindeer		
	4 \times	8 \times	16 \times	4 \times	8 \times	16 \times	4 \times	8 \times	16 \times	4 \times	8 \times	16 \times	4 \times	8 \times	16 \times	4 \times	8 \times	16 \times
Bicubic	3.23	3.98	5.18	2.64	2.81	3.47	2.62	2.81	3.28	2.81	3.13	4.14	2.63	2.82	2.84	2.84	3.18	3.52
GF [39]	1.91	2.87	4.90	1.13	1.84	2.80	1.14	1.86	2.69	1.31	2.12	3.39	1.17	1.87	2.77	1.33	2.10	3.56
DMSG [6]	0.84	1.57	2.98	0.62	1.18	1.48	0.84	1.12	1.78	0.78	1.03	1.89	0.66	1.13	1.76	0.57	1.12	1.87
DGDIE [36]	0.99	1.84	3.34	0.81	1.29	2.04	0.95	1.39	2.05	1.10	1.73	2.67	0.84	1.37	2.16	0.79	1.33	2.19
DSRNet [7]	2.19	2.57	3.69	1.81	1.82	2.16	1.84	1.91	2.21	1.93	2.07	2.66	1.81	1.84	2.26	1.95	2.09	2.59
GSPRT [9]	0.68	1.33	2.47	0.52	0.87	1.37	0.78	1.26	2.03	0.76	1.24	1.86	0.65	1.03	1.68	0.55	1.04	1.70
DJFR [11]	0.91	1.45	2.45	0.86	1.29	1.84	0.94	1.36	1.83	0.97	1.55	2.22	0.76	1.13	1.56	0.70	1.05	1.59
PacNet [8]	0.75	1.22	2.18	0.65	0.98	1.52	0.79	1.14	1.76	0.78	1.24	1.88	0.57	0.85	1.39	0.60	0.91	1.41
CUNet [13]	0.84	1.50	2.83	0.76	1.32	2.04	0.89	1.35	1.96	0.91	1.53	2.58	0.63	0.99	1.69	0.64	1.07	1.91
PMBAN [10]	<u>0.59</u>	<u>0.98</u>	<u>1.89</u>	0.44	0.71	<u>1.23</u>	<u>0.78</u>	<u>1.01</u>	<u>1.56</u>	0.54	<u>0.89</u>	<u>1.62</u>	0.48	<u>0.81</u>	<u>1.30</u>	0.47	<u>0.78</u>	<u>1.52</u>
DKN [12]	0.65	1.04	1.89	0.59	<u>0.90</u>	1.52	0.72	1.03	1.59	0.70	1.08	1.85	0.54	0.79	1.24	<u>0.52</u>	0.79	1.29
AHMF (Ours)	0.56	0.90	1.66	<u>0.49</u>	<u>0.71</u>	1.21	0.65	0.93	1.55	<u>0.57</u>	0.87	1.44	<u>0.49</u>	0.72	1.12	0.47	0.69	1.12

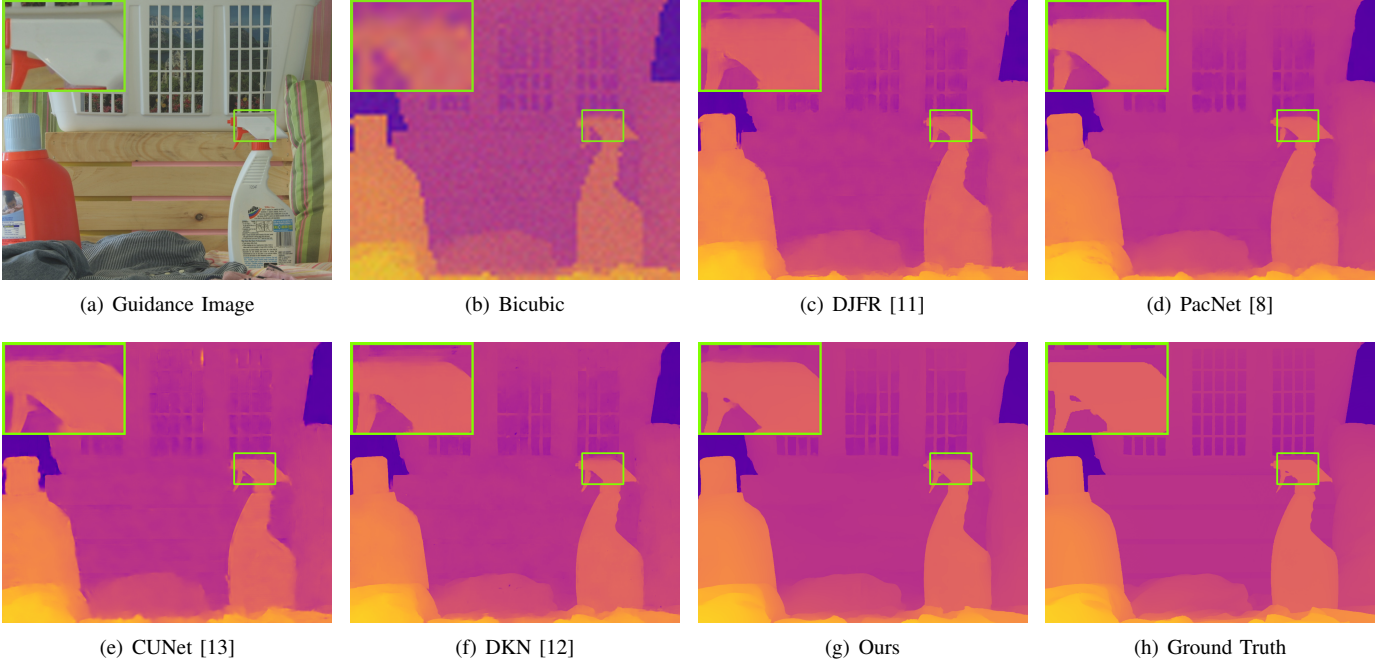


Fig. 6. Visual comparison of $16\times$ results on *Laundry* from Middlebury [38] dataset. Please enlarge the PDF for more details.

where D_{SR} and D_{GT} are network output and ground depth image respectively, N is number of test samples. Note that, for both metrics, lower values indicate better objective quality.

B. Implementation Details

Our model has only one specific hyper-parameter m , which is used to control the number of convolutional layers for multi-modal feature extraction. To balance the efficiency and network performance, we set $m = 4$ as default. The kernel size of a convolutional layer is set as 3×3 , except for those in the upsampling and downsampling module that are set as 1×1 , 3×3 and 5×5 with a stride size of 0, 1, 2 in $4\times$, $8\times$, $16\times$ super-resolution, respectively. The channel number of all the intermediate layers is set as 64. We use PReLU

[32] as the default activation function. During training, we randomly select 16 HR depth maps with the size of 256×256 as the ground truth, the LR depth maps are generated by down-sampling the HR data using bicubic (for Middlebury dataset) or nearest (for NYU v2 dataset) kernel. Our model is optimized by Adam [45] with $\beta_1 = 0.9$, $\beta_2 = 0.999$, and $\epsilon = 1e-8$; the initial learning rate is 1×10^{-4} , then decays to one half at 200 epochs and stops at 250 epochs. The proposed model is implemented by PyTorch [46] and trained on a NVIDIA V100 GPU.

C. Comparison with State-of-the-arts

1) *Experimental Results on Middlebury Dataset (Noiseless Case):* For Middlebury dataset, we compare the proposed

TABLE III

AMAE VALUES FOR SCALE FACTORS $4\times$, $8\times$ AND $16\times$ WITH BICUBIC DEGRADATION ON LU DATASET. THE BEST PERFORMANCE IS SHOWN IN **BOLD** AND SECOND BEST PERFORMANCE IS THE UNDERSCORED ONES (LOWER MAE VALUES, BETTER PERFORMANCE).

Method	Image_01			Image_02			Image_03			Image_04			Image_05			Image_06			Average		
	4 \times	8 \times	16 \times	4 \times	8 \times	16 \times	4 \times	8 \times	16 \times	4 \times	8 \times	16 \times	4 \times	8 \times	16 \times	4 \times	8 \times	16 \times	4 \times	8 \times	16 \times
Bicubic	0.69	1.39	2.50	0.94	2.15	4.43	0.51	1.00	1.90	0.84	1.80	3.48	0.69	1.56	3.15	0.64	1.33	2.67	0.72	1.54	3.02
DSRNet [7]	0.69	1.09	1.94	0.94	1.57	3.17	0.51	0.90	1.61	0.84	1.28	2.57	0.69	1.19	2.21	0.64	0.95	1.94	0.72	1.16	2.24
CUNet [13]	0.57	1.13	2.15	0.78	1.54	3.19	0.51	0.90	1.94	0.61	1.27	2.71	0.57	1.04	2.34	0.54	0.92	1.96	<u>0.60</u>	1.13	2.38
PacNet [8]	0.59	1.01	2.03	0.83	1.39	3.05	0.50	0.90	1.75	<u>0.60</u>	1.13	2.29	0.62	0.97	1.89	0.52	0.87	1.69	0.61	1.05	2.12
DJFR [11]	0.56	0.94	2.00	0.82	1.41	3.05	<u>0.46</u>	0.87	1.68	0.61	1.15	2.24	<u>0.60</u>	0.98	1.96	0.52	0.85	1.50	<u>0.60</u>	1.03	2.07
PMBAN [10]	<u>0.51</u>	<u>0.82</u>	<u>1.67</u>	0.73	<u>1.23</u>	<u>2.53</u>	0.42	0.75	1.31	0.53	<u>0.93</u>	<u>1.94</u>	0.54	0.81	<u>1.60</u>	<u>0.47</u>	<u>0.73</u>	<u>1.29</u>	0.53	<u>0.88</u>	<u>1.72</u>
AHMF (Ours)	0.49	0.81	1.64	0.74	1.18	2.38	0.42	0.77	<u>1.34</u>	0.53	0.90	1.45	0.54	<u>0.84</u>	1.48	0.46	0.69	1.15	0.53	0.86	1.57

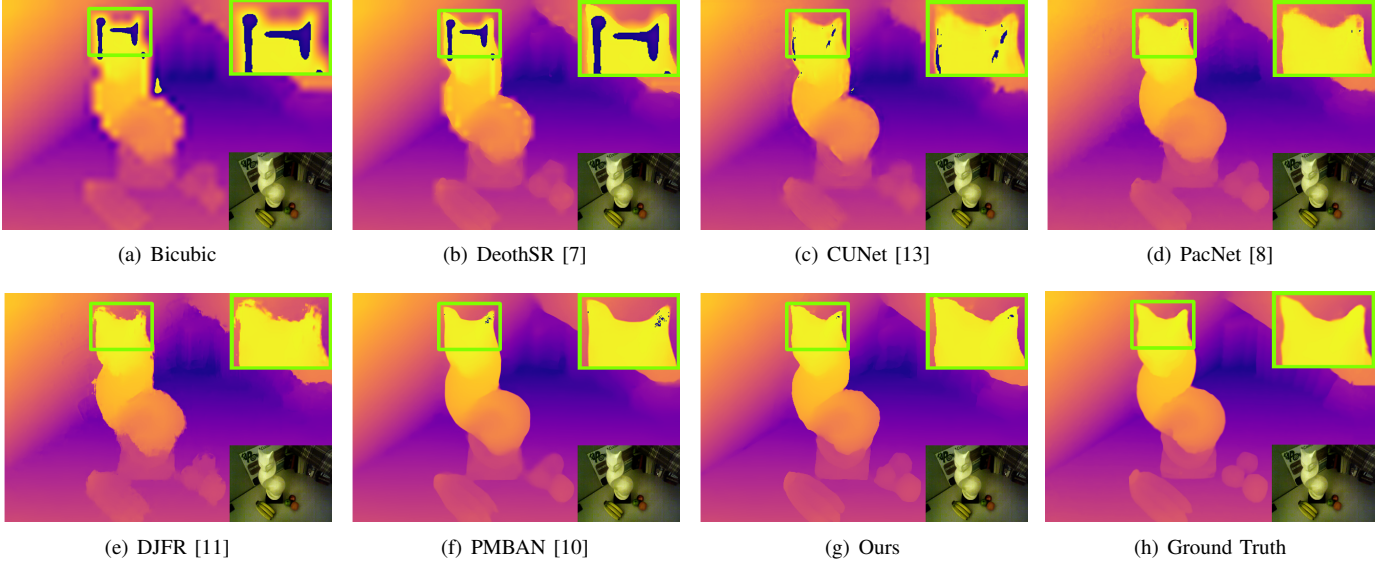


Fig. 7. Visual comparison of $16\times$ results on *Image_06* from Lu dataset [44]. Please enlarge the PDF for more details.

TABLE IV

AVERAGE RMSE PERFORMANCE COMPARISON FOR SCALE FACTORS $4\times$, $8\times$ AND $16\times$ WITH NEAREST-NEIGHBOR DEGRADATION. THE BEST PERFORMANCE IS SHOWN IN **BOLD** AND SECOND BEST PERFORMANCE IS THE UNDERSCORED ONES. FOR NYU [40] WE CALCULATE IN CENTIMETER, FOR OTHER DATASETS WE CALCULATE RMSE WITH DEPTH VALUE SCALED TO $[0, 255]$ (LOWER RMSE VALUES, BETTER PERFORMANCE).

Method	Middlebury [38]			Lu [44]			NYU [40]			Average		
	4 \times	8 \times	16 \times	4 \times	8 \times	16 \times	4 \times	8 \times	16 \times	4 \times	8 \times	16 \times
Bicubic	4.44	7.58	11.87	5.07	9.22	14.27	8.16	14.22	22.32	5.89	10.34	16.15
MRF [47]	4.26	7.43	11.80	4.90	9.03	14.19	7.84	13.98	22.20	5.67	10.15	16.06
GF [39]	4.01	7.22	11.70	4.87	8.85	14.09	7.32	13.62	22.03	5.4	9.90	15.94
TGV [48]	3.39	5.41	12.03	4.48	7.58	17.46	6.98	11.23	28.13	4.95	8.07	19.21
Park [49]	2.82	4.08	7.26	4.09	6.19	10.14	5.21	9.56	18.10	4.04	6.61	11.83
Ham [50]	3.14	5.03	8.83	4.65	7.73	11.52	5.27	12.31	19.24	4.35	8.36	13.20
JBK [14]	2.44	3.81	6.13	2.99	5.06	7.51	4.07	8.29	13.35	3.17	5.72	9.00
DMSG [6]	2.11	3.74	6.03	2.48	4.74	7.51	3.37	6.20	10.05	2.65	4.89	7.86
PacNet [8]	1.91	3.20	5.60	2.48	4.37	6.60	2.82	5.01	8.64	2.40	4.19	6.95
DJFR [11]	1.98	3.61	6.07	<u>2.21</u>	<u>3.75</u>	7.53	3.38	5.86	10.11	2.52	4.41	7.90
FDKN [12]	2.21	3.64	6.15	2.64	4.55	7.20	2.63	4.99	8.67	2.49	4.39	7.34
DKN [12]	<u>1.93</u>	<u>3.17</u>	<u>5.49</u>	2.35	4.16	<u>6.33</u>	<u>2.46</u>	<u>4.76</u>	<u>8.50</u>	<u>2.25</u>	<u>4.03</u>	<u>6.77</u>
AHMF (Ours)	1.77	2.70	5.02	2.00	3.69	6.21	2.21	4.45	8.01	1.99	3.61	6.41

method with 12 state-of-the-art DSR methods: ATGV [35], DMSG [6], DEDIE [36], DSRNet [7], CCFN [37], GSPRT [51], DJFR [11], Pacnet [8], CUNet [13], MDAR [1],

PMBAN [10] and DKN [12]. For fair comparison, we re-train DSRNet [7], DJFR [11], Pacnet [8], CUNet [13] and DKN [12] under the same configurations as ours. The results

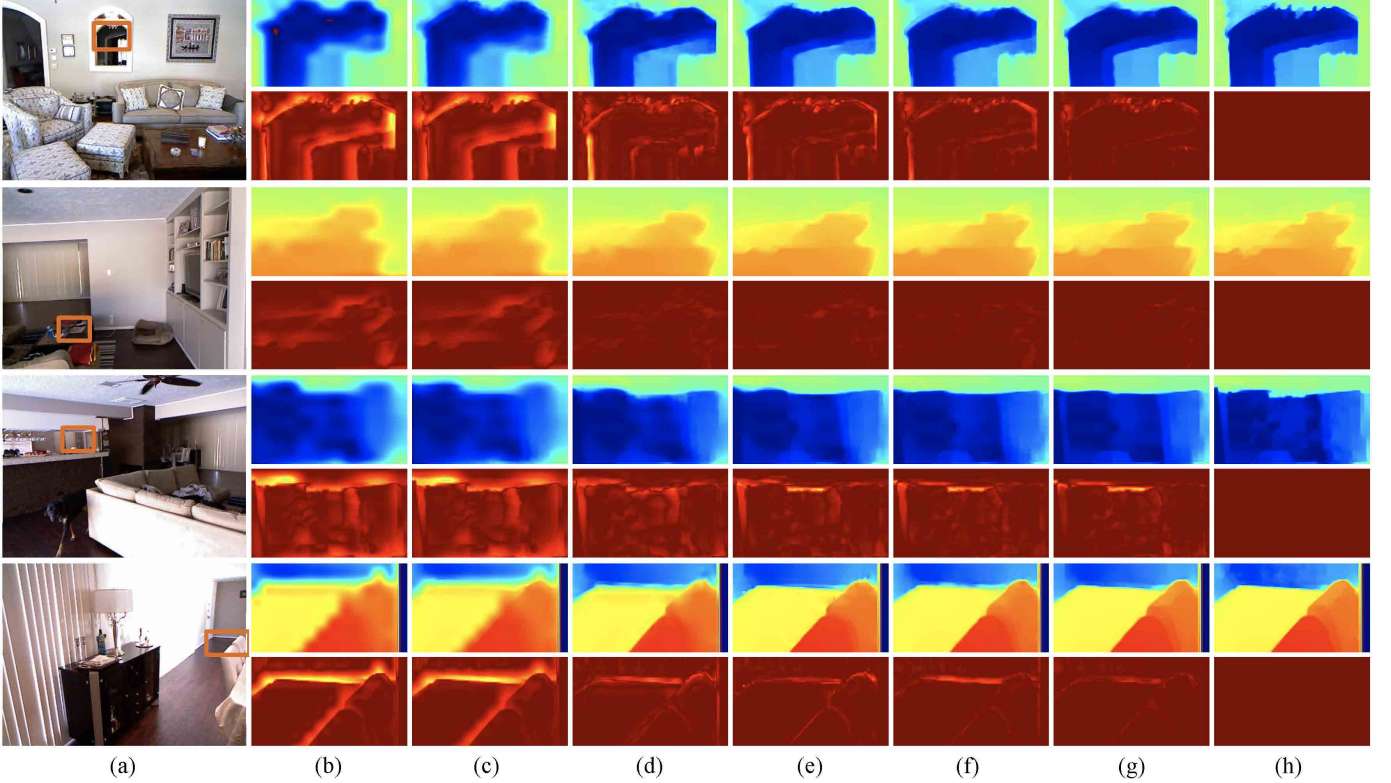


Fig. 8. Visual comparison of $8 \times$ results on *Image_1339*, *Image_1242*, *Image_1241* and *Image_1360* from NYU v2 [40] dataset: (a): Guidance Image, (b): Bicubic, (c): GF [39] (d): DJFR [11], (e): DKN [12], (f): PacNet [8], (g): Ours, (h): GT. For each sample, the second row shows the error map between the results and ground truth. In the error map, brighter area means the larger error. Please enlarge the PDF for more details.

of PMBAN [10] are obtained by its released trained models. Table I lists the results in terms of MAE values at $4 \times$, $8 \times$ and $16 \times$ upsampling of different methods. It can be observed that our method almost obtains the best quantitative scores in all cases, especially for $16 \times$ case which is more difficult to reconstruct.

We also show the zoomed results of various methods in Fig. 5, from which we can see that most of existing approaches cannot generate clear boundaries and suffer from various artifacts. Take Art as an example, the results of DSRNet [7] have texture copy artifacts at the highlighted regions. The results of DJFR [11], PacNet [8] and CUNet [13] cannot generate continuous boundaries of the highlighted pencil region. For PMBAN [10] and DKN [12], both have diffusion artifacts in the region of pencil. In contrast, the proposed method can produce sharp boundaries without diffusion artifacts. We attribute this to the proposed feature fusion and collaboration modules, which fully exploit the relevant information from LR depth and HR guidance.

2) *Experimental Results on Middlebury Dataset (Noisy Case)*: Following [7], [10], we simulate the ToF-like degradation by adding Gaussian noise with standard deviation of 5 to the LR depth maps. Table II shows the MAE comparison results for $4 \times$, $8 \times$ and $16 \times$ upsampling on Middlebury dataset. From this table, it can be found that the proposed method can better deal with the effect of noise when upsampling the depth maps, even compared to the recently proposed deep learning methods, *i.e.*, CUNet [13], PMBAN [10] and

DKN [12]. We further present the qualitative results of $16 \times$ downsampling and noisy degradation in Fig. 6. We can see that our proposed method achieves the clearest and sharpest results. Both PMBAN [10] and DKN [12] generate competitive MAE scores, but suffer from edge blurring artifacts.

3) Evaluation on Generalization Ability across Datasets:

To verify the generalization ability of the proposed method, we test our method on Lu dataset, which is from different resource with the training dataset. The comparison study is conducted with DepthSR [7], CUNet [13], PacNet [8], DJFR [11] and PMBAN [10], which are all trained on the same datasets for fair comparison. As shown in Table III, we can learn that our method constantly obtains the best performances (average MAE values) among compared methods. The visual results in Fig. 7 also demonstrate the superiority of our method. For example, in the head of the toy cat, the results of the compared methods are either seriously distorted or blurred. In contrast, our results are sharper and with least artifacts. This can also demonstrate the advantage of our method.

4) *Experimental Results on NYU v2 Dataset*: To evaluate the effectiveness of the proposed method, we conduct experiments on NYU v2 dataset. We compare our method with DJFR [11], DKN [12] and PacNet [8]. For fairness, we re-train DKN [12] and PacNet [8] with the same training dataset as ours. Since these methods are evaluated by RMSE index in their original papers, we report the RMSE performance in Table IV. Obviously, our method outperforms all compared methods with a large margin. We show visual results at $8 \times$

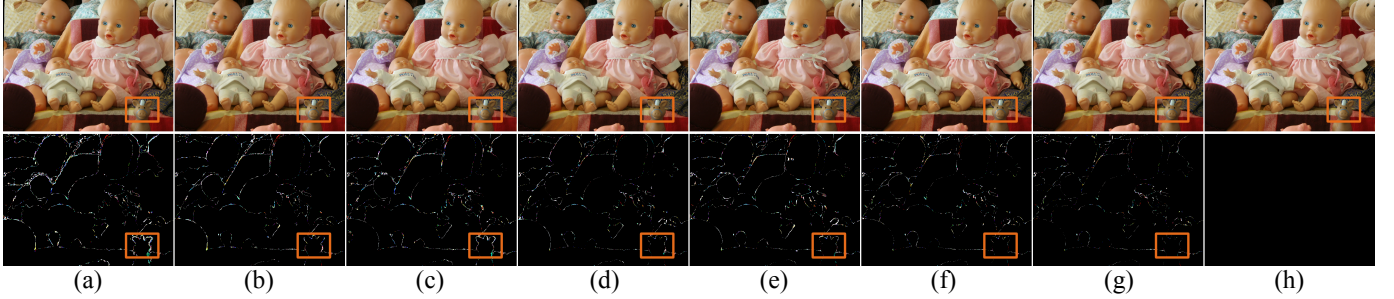


Fig. 9. Visual comparisons of depth image based rendering on *Dolls* from Middlebury [38] dataset: (a): Bicubic, (b): DSRNet [7], (c): DJFR [11], (d): PacNet [8], (e): CUNet [13],(f): PMBAN [10], (g): Ours, (h): GT. The second row shows the error map between the results and ground truth, brighter areas means the larger error. Please enlarge the PDF for more details.

TABLE V
PSNR VALUES FOR DEPTH IMAGE BASED RENDERING.

Method	Art	Books	Dolls	Laundry	Moebius	Reindeer
Bicubic	25.43	32.42	34.33	26.19	32.53	29.76
DSRNet [7]	27.49	33.71	34.65	28.10	33.60	30.00
CUNet [13]	29.78	33.77	35.44	28.00	34.09	33.58
PacNet [8]	31.52	35.08	35.50	30.50	34.85	35.45
DJFR [11]	32.31	35.95	36.72	30.55	35.54	34.37
PMBAN [10]	<u>33.01</u>	<u>37.44</u>	<u>37.14</u>	<u>31.82</u>	<u>35.96</u>	<u>35.98</u>
Ours	34.57	37.87	37.85	32.64	37.22	38.49

upsampling for *Image_1241*, *Image_1242*, *Image_1339* and *Image_1360* in Fig. 8. As can be seen, the results of GF [39] are over-smoothed due to that the local filter cannot capture global information. The results of DJFR [11] and DKN [12] suffer from diffusion artifacts. The result of PacNet [8] can preserve the local details, but cannot reconstruct boundary well. On the contrary, our method is able to produce more precise edges with smaller reconstruction errors than these competing methods.

5) *Experimental Results on Depth Image based Rendering*: Similar to [52], we take depth image based rendering (DIBR) as a measurement to evaluate the performance of the depth SR methods. The stereo depth map used for DIBR is down-sampled by bicubic with $8\times$ scaling factor, then the super-resolved depth maps are used to perform DIBR. Table V tabulates the PSNR values for compared methods on Middlebury dataset. It can be observed that the proposed method achieves the best performance for all test images. We present the visual comparison results and error maps for image *Dolls* in Fig. 9. Obviously, the proposed HMAC method can produce visually appealing results with smaller error maps.

D. Ablation Study

In this section, we conduct ablation studies on Middlebury dataset for $4\times$ upsampling to verify the effectiveness of the proposed multi-modal attention fusion (MMAF) and bi-directional hierarchical feature collaboration (BHFC) module.

In Table VI, Model0 refers to the baseline that only uses concatenation for multi-modal and hierarchical feature fusion. Note that we report the average MAE values of all testing samples.

TABLE VI
ABLATION STUDY OF MULTI-MODAL ATTENTION BASED FUSION (MMAF) AND BI-DIRECTIONAL FEATURE COLLABORATION (BHFC).

	FEB	FRB	Forward	Backward	MAE
Model0	×	×	×	×	0.1750
Model1	✓	×	×	×	0.1730
Model2	×	✓	×	×	0.1721
Model3	✓	✓	×	×	0.1716
Model4	✓	✓	✓	×	0.1714
Model5	✓	✓	×	✓	0.1654
Model6	✓	✓	✓	✓	0.1638

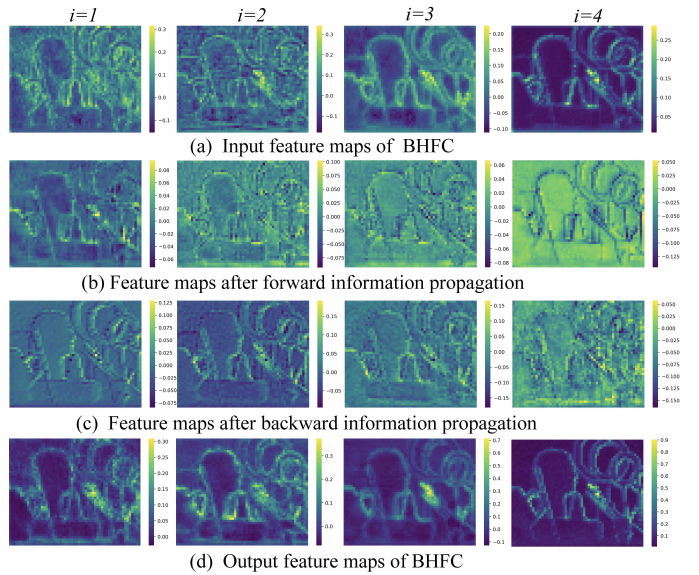


Fig. 10. Average feature maps before and after BHFC, i denotes the i -th layer.

Effect of Multi-modal Attention. The aim of MMAF is to fuse multi-modal features, and it is composed of a feature enhancement block (FEB) and a feature recalibration block (FRB). In Table VI, Model1 to Model3 are used to demonstrate that each component in MMAF can improve the performance over the baseline. When MMAF is completely added, the MAE can be reduced from 0.1750 to 0.1716, which further demonstrates the effectiveness of MMAF for multi-modal feature fusion.

Effect of Hierarchical Feature Collaboration. Model4 to Model6 of Table VI are presented to demonstrate the effectiveness of BHFC. It can be found that although the forward (Model4) and backward (Model5) feature propagation can obtain better performance than Model3, the proposed scheme (*i.e.*, Model6) with bi-directional hierarchical feature collaboration can outperform them with a large margin. This indicates that BHFC plays a significant role in our model.

To further clarify the mechanism of hierarchical feature collaboration, we visualize the average feature maps of BHFC in Fig. 10. Two observations can be obtained. First, the features encoded by different layers have different attributes: shallower features contain rich details while deeper features contain clear structure information (Fig. 10 (a)); Second, our proposed BHFC can propagate information from one layer to all other layers (Fig.10 (b)-(c)), thus the output features of BHFC can maintain both of fine-grained details and clear structure information (Fig.10 (d)). Thanks to this hierarchical feature collaboration mechanism, our proposed method achieves superior performance than the state-of-the-arts.

VII. CONCLUSION

In this paper, we presented a novel attention-based hierarchical multi-modal fusion (AHMF) network for guided depth map super-resolution. It consists of a multi-modal attention based fusion (MMAF) and a bi-directional hierarchical feature collaboration (BHFC) module. The MMAF can effectively select and combine relevant information from multi-modal features extracted from input depth and guidance image in a learning manner. The BHFC is designed for optimizing the use of hierarchical features fused by MMAF with the proposed bi-directional feature propagation and collaboration mechanism. Extensive experiments on widely used benchmark datasets demonstrate that the proposed method can achieve state-of-the-art performance in terms of reconstruction accuracy, inference speed as well as peak GPU memory consumption.

REFERENCES

- [1] H. Hirschmuller and D. Scharstein, “Evaluation of cost functions for stereo matching,” in *Proceedings of the IEEE Conference on Computer Vision and Pattern Recognition*, 2007, pp. 1–8.
- [2] H. Caesar, V. Bankiti, A. H. Lang, S. Vora, V. E. Liang, Q. Xu, A. Krishnan, Y. Pan, G. Baldan, and O. Beijbom, “nuscenes: A multimodal dataset for autonomous driving,” in *Proceedings of the IEEE Conference on Computer Vision and Pattern Recognition*, 2020, pp. 11 621–11 631.
- [3] A. Meuleman, S.-H. Baek, F. Heide, and M. H. Kim, “Single-shot monocular rgb-d imaging using uneven double refraction,” in *Proceedings of the IEEE Conference on Computer Vision and Pattern Recognition*, 2020, pp. 2465–2474.
- [4] J. Hou, A. Dai, and M. Niessner, “3d-sis: 3d semantic instance segmentation of rgb-d scans,” in *Proceedings of the IEEE Conference on Computer Vision and Pattern Recognition*, June 2019.
- [5] D. Lin and H. Huang, “Zig-zag network for semantic segmentation of rgb-d images,” *IEEE Transactions on Pattern Analysis and Machine Intelligence*, vol. 42, no. 10, pp. 2642–2655, 2020.
- [6] T.-W. Hui, C. C. Loy, and X. Tang, “Depth map super-resolution by deep multi-scale guidance,” in *Proceedings of the European Conference on Computer Vision*, 2016.
- [7] C. Guo, C. Li, J. Guo, R. Cong, H. Fu, and P. Han, “Hierarchical features driven residual learning for depth map super-resolution,” *IEEE Transactions on Image Processing*, vol. 28, no. 5, pp. 2545–2557, 2019.
- [8] H. Su, V. Jampani, D. Sun, O. Gallo, E. Learned-Miller, and J. Kautz, “Pixel-adaptive convolutional neural networks,” in *Proceedings of the IEEE Conference on Computer Vision and Pattern Recognition*, 2019.
- [9] R. d. Lutio, S. D’aronco, J. D. Wegner, and K. Schindler, “Guided super-resolution as pixel-to-pixel transformation,” in *Proceedings of the IEEE International Conference on Computer Vision*, 2019, pp. 8829–8837.
- [10] X. Ye, B. Sun, Z. Wang, J. Yang, R. Xu, H. Li, and B. Li, “Pmabanet: Progressive multi-branch aggregation network for scene depth super-resolution,” *IEEE Transactions on Image Processing*, vol. 29, pp. 7427–7442, 2020.
- [11] Y. Li, J. B. Huang, N. Ahuja, and M. H. Yang, “Joint image filtering with deep convolutional networks,” *IEEE Transactions on Pattern Analysis and Machine Intelligence*, vol. 41, no. 8, pp. 1909–1923, 2019.
- [12] B. Kim, J. Ponce, and B. Ham, “Deformable kernel networks for joint image filtering,” *International Journal of Computer Vision*, pp. 1–22, 2020.
- [13] X. Deng and P. L. Dragotti, “Deep convolutional neural network for multi-modal image restoration and fusion,” *IEEE Transactions on Pattern Analysis and Machine Intelligence*, 2020.
- [14] J. Kopf, M. F. Cohen, D. Lischinski, and M. Uyttendaele, “Joint bilateral upsampling,” *AcM Transactions on Graphics*, vol. 26, no. 3, pp. 96.1–96.4, 2007.
- [15] M. Liu, O. Tuzel, and Y. Taguchi, “Joint geodesic upsampling of depth images,” in *Proceedings of the IEEE Conference on Computer Vision and Pattern Recognition*, 2013, pp. 169–176.
- [16] D. Ferstl, C. Reinbacher, R. Ranftl, M. Ruehrt, and H. Bischof, “Image guided depth upsampling using anisotropic total generalized variation,” in *Proceedings of the IEEE International Conference on Computer Vision*, 2013.
- [17] X. Liu, D. Zhai, R. Chen, X. Ji, D. Zhao, and W. Gao, “Depth restoration from rgb-d data via joint adaptive regularization and thresholding on manifolds,” *IEEE Transactions on Image Processing*, vol. 28, no. 3, pp. 1068–1079, 2019.
- [18] C. Guo, C. Li, J. Guo, R. Cong, H. Fu, and P. Han, “Hierarchical features driven residual learning for depth map super-resolution,” *IEEE Transactions on Image Processing*, vol. 28, no. 5, pp. 2545–2557, 2019.
- [19] H. Zhang, I. Goodfellow, D. Metaxas, and A. Odena, “Self-attention generative adversarial networks,” in *Proceedings of the 36th International Conference on Machine Learning*, ser. Proceedings of Machine Learning Research, K. Chaudhuri and R. Salakhutdinov, Eds., vol. 97. Long Beach, California, USA: PMLR, 09–15 Jun 2019, pp. 7354–7363.
- [20] X. Wang, R. Girshick, A. Gupta, and K. He, “Non-local neural networks,” in *Proceedings of the IEEE/CVF Conference on Computer Vision and Pattern Recognition*, 2018, pp. 7794–7803.
- [21] J. Hu, L. Shen, S. Albanie, G. Sun, and E. Wu, “Squeeze-and-excitation networks,” *IEEE Transactions on Pattern Analysis and Machine Intelligence*, 2017.
- [22] X. Li, W. Wang, X. Hu, and J. Yang, “Selective kernel networks,” in *Proceedings of the IEEE Conference on Computer Vision and Pattern Recognition (CVPR)*, June 2019.
- [23] Y. Mei, Y. Fan, Y. Zhang, J. Yu, Y. Zhou, D. Liu, Y. Fu, T. S. Huang, and H. Shi, “Pyramid attention networks for image restoration,” *arXiv preprint arXiv:2004.13824*, 2020.
- [24] Q. Wang, B. Wu, P. Zhu, W. Z. Peihua Li, and Q. Hu, “Eca-net: Efficient channel attention for deep convolutional neural networks,” in *Proceedings of the IEEE Conference on Computer Vision and Pattern Recognition (CVPR)*, 2020.
- [25] J. Yu, Z. Lin, J. Yang, X. Shen, X. Lu, and T. Huang, “Free-form image inpainting with gated convolution,” in *Proceedings of the IEEE International Conference on Computer Vision (ICCV)*, 2019, pp. 4470–4479.
- [26] Y. Chang, Z. Y. Liu, K. Lee, and W. Hsu, “Free-form video inpainting with 3d gated convolution and temporal patchgan,” in *Proceedings of the IEEE/CVF International Conference on Computer Vision (ICCV)*, 2019, pp. 9065–9074.
- [27] K. He, X. Zhang, S. Ren, and J. Sun, “Deep residual learning for image recognition,” in *Proceedings of the IEEE Conference on Computer Vision and Pattern Recognition (CVPR)*, 2016, pp. 770–778.
- [28] G. Huang, Z. Liu, L. Van Der Maaten, and K. Q. Weinberger, “Densely connected convolutional networks,” in *Proceedings of the IEEE Conference on Computer Vision and Pattern Recognition (CVPR)*, 2017, pp. 2261–2269.
- [29] S. Gu, Y. Li, L. V. Gool, and R. Timofte, “Self-guided network for fast image denoising,” in *Proceedings of the IEEE International Conference on Computer Vision (ICCV)*, October 2019.
- [30] G. Lin, F. Liu, A. Milan, C. Shen, and I. Reid, “Refinenet: Multi-path refinement networks for dense prediction,” *IEEE Transactions on Pattern Analysis and Machine Intelligence*, 2019.

[31] J. Kwak and D. Son, "Fractal residual network and solutions for real super-resolution," in *Proceedings of IEEE/CVF Conference on Computer Vision and Pattern Recognition Workshops (CVPRW)*, 2019, pp. 2114–2121.

[32] K. He, X. Zhang, S. Ren, and J. Sun, "Delving deep into rectifiers: Surpassing human-level performance on imagenet classification," in *Proceedings of the IEEE International Conference on Computer Vision*, 2015, pp. 1026–1034.

[33] W. Shi, J. Caballero, F. Huszár, J. Totz, A. P. Aitken, R. Bishop, D. Rueckert, and Z. Wang, "Real-time single image and video super-resolution using an efficient sub-pixel convolutional neural network," in *Proceedings of the IEEE Conference on Computer Vision and Pattern Recognition*, 2016, pp. 1874–1883.

[34] B. Lim, S. Son, H. Kim, S. Nah, and K. Mu Lee, "Enhanced deep residual networks for single image super-resolution," in *Proceedings of the IEEE Conference on Computer Vision and Pattern Recognition workshops*, 2017, pp. 136–144.

[35] G. Riegler, M. Rüther, and H. Bischof, "Atgv-net: Accurate depth super-resolution," in *Proceedings of the European conference on computer vision*. Springer, 2016, pp. 268–284.

[36] S. Gu, W. Zuo, S. Guo, Y. Chen, C. Chen, and L. Zhang, "Learning dynamic guidance for depth image enhancement," in *Proceedings of the IEEE Conference on Computer Vision and Pattern Recognition*, 2017, pp. 3769–3778.

[37] Y. Wen, B. Sheng, P. Li, W. Lin, and D. D. Feng, "Deep color guided coarse-to-fine convolutional network cascade for depth image super-resolution," *IEEE Transactions on Image Processing*, vol. 28, no. 2, pp. 994–1006, 2019.

[38] D. Scharstein and C. Pal, "Learning conditional random fields for stereo," in *Proceedings of the IEEE Conference on Computer Vision and Pattern Recognition*. IEEE, 2007, pp. 1–8.

[39] K. He, J. Sun, and X. Tang, "Guided image filtering," *IEEE Transactions on Pattern Analysis & Machine Intelligence*, vol. 35, no. 6, pp. 1397–1409, 2013.

[40] N. Silberman, D. Hoiem, P. Kohli, and R. Fergus, "Indoor segmentation and support inference from rgbd images," in *Proceedings of the 12th European Conference on Computer Vision - Volume Part V*, 2012.

[41] D. J. Butler, J. Wulff, G. B. Stanley, and M. J. Black, "A naturalistic open source movie for optical flow evaluation," in *Proceedings of the European Conference on Computer Vision*. Springer, 2012, pp. 611–625.

[42] S. Baker, D. Scharstein, J. Lewis, S. Roth, M. J. Black, and R. Szeliski, "A database and evaluation methodology for optical flow," *International Journal of Computer Vision*, vol. 92, no. 1, pp. 1–31, 2011.

[43] D. Scharstein, H. Hirschmüller, Y. Kitajima, G. Krathwohl, N. Nešić, X. Wang, and P. Westling, "High-resolution stereo datasets with subpixel-accurate ground truth," in *German Conference on Pattern Recognition*. Springer, 2014, pp. 31–42.

[44] S. Lu, X. Ren, and F. Liu, "Depth enhancement via low-rank matrix completion," in *Proceedings of the IEEE Conference on Computer Vision and Pattern Recognition*, 2014, pp. 3390–3397.

[45] D. P. Kingma and J. Ba, "Adam: A method for stochastic optimization," *arXiv: Learning*, 2014.

[46] A. Paszke, S. Gross, S. Chintala, G. Chanan, E. Yang, Z. DeVito, Z. Lin, A. Desmaison, L. Antiga, and A. Lerer, "Automatic differentiation in pytorch," 2017.

[47] J. Diebel and S. Thrun, "An application of markov random fields to range sensing," *Advances in Neural Information Processing Systems*, pp. 291–298, 2005.

[48] D. Ferstl, C. Reinbacher, R. Ranftl, M. Rüther, and H. Bischof, "Image guided depth upsampling using anisotropic total generalized variation," in *Proceedings of the IEEE International Conference on Computer Vision*, 2013, pp. 993–1000.

[49] J. Park, H. Kim, Y. W. Tai, M. S. Brown, and I. Kweon, "High quality depth map upsampling for 3d-tof cameras," in *IEEE International Conference on Computer Vision*, 2011.

[50] B. Ham, M. Cho, and J. Ponce, "Robust image filtering using joint static and dynamic guidance," in *Computer Vision & Pattern Recognition*, 2015.

[51] R. D. Lutio, S. D'aronco, J. D. Wegner, and K. Schindler, "Guided super-resolution as pixel-to-pixel transformation," in *Proceedings of the IEEE/CVF International Conference on Computer Vision (ICCV)*, 2019, pp. 8828–8836.

[52] Y. Zhang, Y. Feng, X. Liu, D. Zhai, X. Ji, H. Wang, and Q. Dai, "Color-guided depth image recovery with adaptive data fidelity and transferred graph laplacian regularization," *IEEE Transactions on Circuits and Systems for Video Technology*, vol. 30, no. 2, pp. 320–333, 2019.

REFERENCES

[1] H. Hirschmüller and D. Scharstein, "Evaluation of cost functions for stereo matching," in *Proceedings of the IEEE Conference on Computer Vision and Pattern Recognition*, 2007, pp. 1–8.

[2] H. Caesar, V. Bankiti, A. H. Lang, S. Vora, V. E. Liou, Q. Xu, A. Krishnan, Y. Pan, G. Baldan, and O. Beijbom, "nuscenes: A multimodal dataset for autonomous driving," in *Proceedings of the IEEE Conference on Computer Vision and Pattern Recognition*, 2020, pp. 11621–11631.

[3] A. Meuleman, S.-H. Baek, F. Heide, and M. H. Kim, "Single-shot monocular rgbd imaging using uneven double refraction," in *Proceedings of the IEEE Conference on Computer Vision and Pattern Recognition*, 2020, pp. 2465–2474.

[4] J. Hou, A. Dai, and M. Niessner, "3d-sis: 3d semantic instance segmentation of rgbd scans," in *Proceedings of the IEEE Conference on Computer Vision and Pattern Recognition*, June 2019.

[5] D. Lin and H. Huang, "Zig-zag network for semantic segmentation of rgbd images," *IEEE Transactions on Pattern Analysis and Machine Intelligence*, vol. 42, no. 10, pp. 2642–2655, 2020.

[6] T.-W. Hui, C. C. Loy, and X. Tang, "Depth map super-resolution by deep multi-scale guidance," in *Proceedings of the European Conference on Computer Vision*, 2016.

[7] C. Guo, C. Li, J. Guo, R. Cong, H. Fu, and P. Han, "Hierarchical features driven residual learning for depth map super-resolution," *IEEE Transactions on Image Processing*, vol. 28, no. 5, pp. 2545–2557, 2019.

[8] H. Su, V. Jampani, D. Sun, O. Gallo, E. Learned-Miller, and J. Kautz, "Pixel-adaptive convolutional neural networks," in *Proceedings of the IEEE Conference on Computer Vision and Pattern Recognition*, 2019.

[9] R. d. Lutio, S. D'aronco, J. D. Wegner, and K. Schindler, "Guided super-resolution as pixel-to-pixel transformation," in *Proceedings of the IEEE International Conference on Computer Vision*, 2019, pp. 8829–8837.

[10] X. Ye, B. Sun, Z. Wang, J. Yang, R. Xu, H. Li, and B. Li, "Pmbanet: Progressive multi-branch aggregation network for scene depth super-resolution," *IEEE Transactions on Image Processing*, vol. 29, pp. 7427–7442, 2020.

[11] Y. Li, J. B. Huang, N. Ahuja, and M. H. Yang, "Joint image filtering with deep convolutional networks," *IEEE Transactions on Pattern Analysis and Machine Intelligence*, vol. 41, no. 8, pp. 1909–1923, 2019.

[12] B. Kim, J. Ponce, and B. Ham, "Deformable kernel networks for joint image filtering," *International Journal of Computer Vision*, pp. 1–22, 2020.

[13] X. Deng and P. L. Dragotti, "Deep convolutional neural network for multi-modal image restoration and fusion," *IEEE Transactions on Pattern Analysis and Machine Intelligence*, 2020.

[14] J. Kopf, M. F. Cohen, D. Lischinski, and M. Uyttendaele, "Joint bilateral upsampling," *AcM Transactions on Graphics*, vol. 26, no. 3, pp. 96.1–96.4, 2007.

[15] M. Liu, O. Tuzel, and Y. Taguchi, "Joint geodesic upsampling of depth images," in *Proceedings of the IEEE Conference on Computer Vision and Pattern Recognition*, 2013, pp. 169–176.

[16] D. Ferstl, C. Reinbacher, R. Ranftl, M. Ruether, and H. Bischof, "Image guided depth upsampling using anisotropic total generalized variation," in *Proceedings of the IEEE International Conference on Computer Vision*, 2013.

[17] X. Liu, D. Zhai, R. Chen, X. Ji, D. Zhao, and W. Gao, "Depth restoration from rgbd data via joint adaptive regularization and thresholding on manifolds," *IEEE Transactions on Image Processing*, vol. 28, no. 3, pp. 1068–1079, 2019.

[18] C. Guo, C. Li, J. Guo, R. Cong, H. Fu, and P. Han, "Hierarchical features driven residual learning for depth map super-resolution," *IEEE Transactions on Image Processing*, vol. 28, no. 5, pp. 2545–2557, 2019.

[19] H. Zhang, I. Goodfellow, D. Metaxas, and A. Odena, "Self-attention generative adversarial networks," in *Proceedings of the 36th International Conference on Machine Learning*, ser. Proceedings of Machine Learning Research, K. Chaudhuri and R. Salakhutdinov, Eds., vol. 97. Long Beach, California, USA: PMLR, 09–15 Jun 2019, pp. 7354–7363.

[20] X. Wang, R. Girshick, A. Gupta, and K. He, "Non-local neural networks," in *Proceedings of the IEEE/CVF Conference on Computer Vision and Pattern Recognition*, 2018, pp. 7794–7803.

[21] J. Hu, L. Shen, S. Albanie, G. Sun, and E. Wu, "Squeeze-and-excitation networks," *IEEE Transactions on Pattern Analysis and Machine Intelligence*, 2017.

[22] X. Li, W. Wang, X. Hu, and J. Yang, "Selective kernel networks," in *Proceedings of the IEEE Conference on Computer Vision and Pattern Recognition (CVPR)*, June 2019.

[23] Y. Mei, Y. Fan, Y. Zhang, J. Yu, Y. Zhou, D. Liu, Y. Fu, T. S. Huang, and H. Shi, "Pyramid attention networks for image restoration," *arXiv preprint arXiv:2004.13824*, 2020.

[24] Q. Wang, B. Wu, P. Zhu, W. Z. Peihua Li, and Q. Hu, "Eca-net: Efficient channel attention for deep convolutional neural networks," in *Proceedings of the IEEE Conference on Computer Vision and Pattern Recognition (CVPR)*, 2020.

[25] J. Yu, Z. Lin, J. Yang, X. Shen, X. Lu, and T. Huang, "Free-form image inpainting with gated convolution," in *Proceedings of the IEEE International Conference on Computer Vision (ICCV)*, 2019, pp. 4470–4479.

[26] Y. Chang, Z. Y. Liu, K. Lee, and W. Hsu, "Free-form video inpainting with 3d gated convolution and temporal patchgan," in *Proceedings of the IEEE/CVF International Conference on Computer Vision (ICCV)*, 2019, pp. 9065–9074.

[27] K. He, X. Zhang, S. Ren, and J. Sun, "Deep residual learning for image recognition," in *Proceedings of the IEEE Conference on Computer Vision and Pattern Recognition (CVPR)*, 2016, pp. 770–778.

[28] G. Huang, Z. Liu, L. Van Der Maaten, and K. Q. Weinberger, "Densely connected convolutional networks," in *Proceedings of the IEEE Conference on Computer Vision and Pattern Recognition (CVPR)*, 2017, pp. 2261–2269.

[29] S. Gu, Y. Li, L. V. Gool, and R. Timofte, "Self-guided network for fast image denoising," in *Proceedings of the IEEE International Conference on Computer Vision (ICCV)*, October 2019.

[30] G. Lin, F. Liu, A. Milan, C. Shen, and I. Reid, "Refinenet: Multi-path refinement networks for dense prediction," *IEEE Transactions on Pattern Analysis and Machine Intelligence*, 2019.

[31] J. Kwak and D. Son, "Fractal residual network and solutions for real super-resolution," in *Proceedings of IEEE/CVF Conference on Computer Vision and Pattern Recognition Workshops (CVPRW)*, 2019, pp. 2114–2121.

[32] K. He, X. Zhang, S. Ren, and J. Sun, "Delving deep into rectifiers: Surpassing human-level performance on imagenet classification," in *Proceedings of the IEEE International Conference on Computer Vision*, 2015, pp. 1026–1034.

[33] W. Shi, J. Caballero, F. Huszár, J. Totz, A. P. Aitken, R. Bishop, D. Rueckert, and Z. Wang, "Real-time single image and video super-resolution using an efficient sub-pixel convolutional neural network," in *Proceedings of the IEEE Conference on Computer Vision and Pattern Recognition*, 2016, pp. 1874–1883.

[34] B. Lim, S. Son, H. Kim, S. Nah, and K. Mu Lee, "Enhanced deep residual networks for single image super-resolution," in *Proceedings of the IEEE Conference on Computer Vision and Pattern Recognition Workshops*, 2017, pp. 136–144.

[35] G. Riegler, M. Rüther, and H. Bischof, "Atgv-net: Accurate depth super-resolution," in *Proceedings of the European conference on computer vision*. Springer, 2016, pp. 268–284.

[36] S. Gu, W. Zuo, S. Guo, Y. Chen, C. Chen, and L. Zhang, "Learning dynamic guidance for depth image enhancement," in *Proceedings of the IEEE Conference on Computer Vision and Pattern Recognition*, 2017, pp. 3769–3778.

[37] Y. Wen, B. Sheng, P. Li, W. Lin, and D. D. Feng, "Deep color guided coarse-to-fine convolutional network cascade for depth image super-resolution," *IEEE Transactions on Image Processing*, vol. 28, no. 2, pp. 994–1006, 2019.

[38] D. Scharstein and C. Pal, "Learning conditional random fields for stereo," in *Proceedings of the IEEE Conference on Computer Vision and Pattern Recognition*. IEEE, 2007, pp. 1–8.

[39] K. He, J. Sun, and X. Tang, "Guided image filtering," *IEEE Transactions on Pattern Analysis & Machine Intelligence*, vol. 35, no. 6, pp. 1397–1409, 2013.

[40] N. Silberman, D. Hoiem, P. Kohli, and R. Fergus, "Indoor segmentation and support inference from rgbd images," in *Proceedings of the 12th European Conference on Computer Vision - Volume Part V*, 2012.

[41] D. J. Butler, J. Wulff, G. B. Stanley, and M. J. Black, "A naturalistic open source movie for optical flow evaluation," in *Proceedings of the European Conference on Computer Vision*. Springer, 2012, pp. 611–625.

[42] S. Baker, D. Scharstein, J. Lewis, S. Roth, M. J. Black, and R. Szeliski, "A database and evaluation methodology for optical flow," *International Journal of Computer Vision*, vol. 92, no. 1, pp. 1–31, 2011.

[43] D. Scharstein, H. Hirschmüller, Y. Kitajima, G. Krathwohl, N. Nešić, X. Wang, and P. Westling, "High-resolution stereo datasets with subpixel-accurate ground truth," in *German Conference on Pattern Recognition*. Springer, 2014, pp. 31–42.

[44] S. Lu, X. Ren, and F. Liu, "Depth enhancement via low-rank matrix completion," in *Proceedings of the IEEE Conference on Computer Vision and Pattern Recognition*, 2014, pp. 3390–3397.

[45] D. P. Kingma and J. Ba, "Adam: A method for stochastic optimization," *arXiv: Learning*, 2014.

[46] A. Paszke, S. Gross, S. Chintala, G. Chanan, E. Yang, Z. DeVito, Z. Lin, A. Desmaison, L. Antiga, and A. Lerer, "Automatic differentiation in pytorch," 2017.

[47] J. Diebel and S. Thrun, "An application of markov random fields to range sensing," *Advances in Neural Information Processing Systems*, pp. 291–298, 2005.

[48] D. Ferstl, C. Reinbacher, R. Ranftl, M. Rüther, and H. Bischof, "Image guided depth upsampling using anisotropic total generalized variation," in *Proceedings of the IEEE International Conference on Computer Vision*, 2013, pp. 993–1000.

[49] J. Park, H. Kim, Y. W. Tai, M. S. Brown, and I. Kweon, "High quality depth map upsampling for 3d-tof cameras," in *IEEE International Conference on Computer Vision*, 2011.

[50] B. Ham, M. Cho, and J. Ponce, "Robust image filtering using joint static and dynamic guidance," in *Computer Vision & Pattern Recognition*, 2015.

[51] R. D. Lutio, S. D'arconco, J. D. Wegner, and K. Schindler, "Guided super-resolution as pixel-to-pixel transformation," in *Proceedings of the IEEE/CVF International Conference on Computer Vision (ICCV)*, 2019, pp. 8828–8836.

[52] Y. Zhang, Y. Feng, X. Liu, D. Zhai, X. Ji, H. Wang, and Q. Dai, "Color-guided depth image recovery with adaptive data fidelity and transferred graph laplacian regularization," *IEEE Transactions on Circuits and Systems for Video Technology*, vol. 30, no. 2, pp. 320–333, 2019.